Original Article

Mitigating Distance Relay Maloperations during Load Encroachment through an Adaptive Mho Distance Relaying Scheme Based on Sequence Components

Sujitha Arasu[1], Rathinam Ananthanarayanan[2]

[1,2]*Department of Electrical and Electronics Engineering, SRM Institute of Science and Technology, Chennai, India.*

[2]*Corresponding Author : rathinaa@srmist.edu.in*

Abstract - Distance relays are critical in safeguarding the electrical grid by detecting faults and maintaining system stability and reliability. However, maloperations can occur under specific conditions, resulting in inaccurate tripping or failure to trip during fault events. This manuscript focuses on developing an adaptive sequence components-based Mho distance relaying scheme to prevent maloperations of distance relays during load encroachment. The proposed scheme incorporates the analysis of sequence components to enhance the accuracy and reliability of fault detection during load encroachment conditions. The scheme effectively prevents maloperations and ensures proper relay operation by adapting the Mho characteristic based on the sequence components and power factor angles. Extensive simulations and testing are conducted using MATLAB/Simulink to validate the proposed scheme's performance in the EMTP-RV environment. The results demonstrate improved fault detection capabilities and reduced maloperations compared to conventional distance relaying schemes. The proposed scheme offers a practical solution to enhance the performance and reliability of distance relays in power systems, particularly during load encroachment conditions.

Keywords - Protective relay, Load encroachment, Ground distance multiplier, Power flow angle, Zero sequence components, Fault resistance.

1. Introduction

The rapid growth of power systems in India has led to an increased reliance on distance relays for fault detection and protection. Distance relays are designed to measure the impedance between the relay location and the fault point, enabling them to detect faults and initiate appropriate corrective actions accurately. However, the maloperation of distance relays can pose significant risks to the power system, resulting in unnecessary tripping or failure to isolate faults.

Distance relays operate based on assumptions about fault characteristics, such as fault resistance, fault location accuracy, and fault impedance. Deviations from these assumptions can result in maloperations. Common factors contributing to maloperations include low fault currents, high fault resistances, or unusual locations [1]. Rapid changes in power system dynamics, such as voltage fluctuations, load variations, and network configuration changes, can impact the performance of distance relays. These dynamic conditions may introduce errors in distance measurements and lead to maloperations [2, 3]. High-frequency transients associated with faults, such as travelling waves, can affect distance relay operations. Signal distortions caused by fault transients can lead to incorrect measurements and subsequent maloperations [4]. Inadequate communication infrastructure or relay coordination can result in maloperations. Communication delays, data corruption, or miscoordination among protective relays can undermine the accurate operation of distance relays [5]. The impacts of distance relay maloperation are explored as Erroneous tripping or failure to trip during fault events can lead to grid instability. This instability can propagate, causing widespread power outages, equipment damage, and potential safety hazards [6, 7].

Distance relay maloperations can result in unnecessary tripping of healthy circuits, leading to disruptions in power supply. These disruptions can have severe economic consequences, including production losses, revenue reduction, and increased maintenance costs [8, 9]. Maloperations impose operational challenges on power system operators. Identifying the cause of the maloperation, locating the fault, and restoring power promptly can be complex and time-consuming, further worsening the impact on the power system [10].

Several studies have explored the use of advanced fault detection techniques to mitigate distance relay maloperation [11-14]. For instance, the study by Gupta et al. proposed a fault classification algorithm based on wavelet packet decomposition and neural network classifiers, achieving accurate fault detection and reducing maloperations [15].

In the study by Bhattacharya et al., published in the IEEE transactions on power delivery, a fault detection algorithm based on wavelet packet decomposition and support vector machines was proposed [16]. The algorithm achieved accurate fault detection and reduced maloperations by effectively capturing fault characteristics. Additionally, the work by Mishra et al. investigated the application of adaptive algorithms for fault detection, highlighting their effectiveness in reducing maloperations caused by system dynamics and fault transients [17].

System modelling and simulation studies are essential for identifying vulnerabilities and optimizing protection schemes to mitigate distance relay maloperation. The study by Sharma et al. focused on developing a comprehensive system model for power system analysis, identifying fault-prone areas and improving relay coordination to minimize maloperations [18].

In the work by Singh et al. published in the IEEE transactions on power systems, a comprehensive system model was developed to analyze the performance of distance relays under various fault conditions. The study demonstrated the significance of system modelling in identifying vulnerable areas and improving relay coordination to minimize maloperations [19]. Similarly, the research by Verma et al. utilized simulation studies to evaluate different fault scenarios and propose enhanced protection schemes to mitigate distance relay maloperation [20]. Selecting appropriate parameters, such as thresholds and time settings, is crucial for the success of these strategies. These parameters must be carefully chosen based on system characteristics to ensure accurate fault detection while minimizing false alarms.

Communication infrastructure is crucial in ensuring accurate relay coordination and mitigating maloperations. Studies have highlighted the importance of communication infrastructure upgrades in mitigating distance relay maloperation [21, 22]. The work by Jain et al. emphasized the implementation of real-time monitoring systems and fibre-optic networks to improve communication speed and reliability, reducing the risk of miscoordination and subsequent maloperations [23].

The research by Sharma et al., published in the IEEE transactions on smart grid, investigated the implementation of real-time monitoring systems and advanced communication networks [24]. The study highlighted the importance of enhanced communication infrastructure in reducing miscoordination and subsequent maloperations. Access to comprehensive and representative fault data for training advanced fault detection techniques can also be challenging, especially in real-world power systems.

Relay coordination and testing are vital for minimizing maloperations caused by inadequate coordination or incorrect relay settings. The study by Aggarwal et al. focused on relay coordination techniques using genetic algorithms, ensuring optimal relay settings and improved coordination, thereby reducing maloperations [25]. Additionally, the work by Sharma et al. emphasized the importance of regular relay testing and maintenance to identify and rectify potential malfunctions, enhancing relay performance and minimizing maloperations [26].

Fault discrimination is a critical aspect of distance relay protection systems in power systems. The papers discuss the complexities arising from fault types, fault impedance, fault resistance, and other system conditions that affect discrimination accuracy [27-32]. It also explores novel techniques, including pattern recognition algorithms, adaptive relaying schemes, and intelligent decision-making approaches, to improve fault discrimination capabilities and enhance the reliability of distance relay protection. Inspite of various schemes available to enhance the robustness and durability.

To overcome the significant disadvantages associated with existing algorithms and effectively discriminate between different types of faults and load encroachment situations, an adaptive Mho distance relaying methodology based on sequence components is proposed.

This paper utilizes a modified Mho characteristic to make the relay more sensitive to high resistance faults and less sensitive to heavy loads. The proposed methodology incorporates modified Mho settings that block the trip signal to address heavy load conditions. Additionally, it considers the encroachment of load impedance in both the modified Mho settings and zone 3. The zero sequence components of fault currents are employed to achieve proper coordination and prevent such situations. The proposed algorithm distinguishes between load encroachment and faulty situations by analyzing the measured impedance trajectory observed by the relay within the loading region.

Additionally, the scheme integrates real-time load impedance monitoring to facilitate timely adjustments and prevent false tripping. The effectiveness of the proposed methodology is validated through various experiments conducted on a heavily loaded long transmission system. The protection system is modelled in MATLAB/Simulink to validate the effectiveness of the pilot scheme in an EMTP-RV environment.
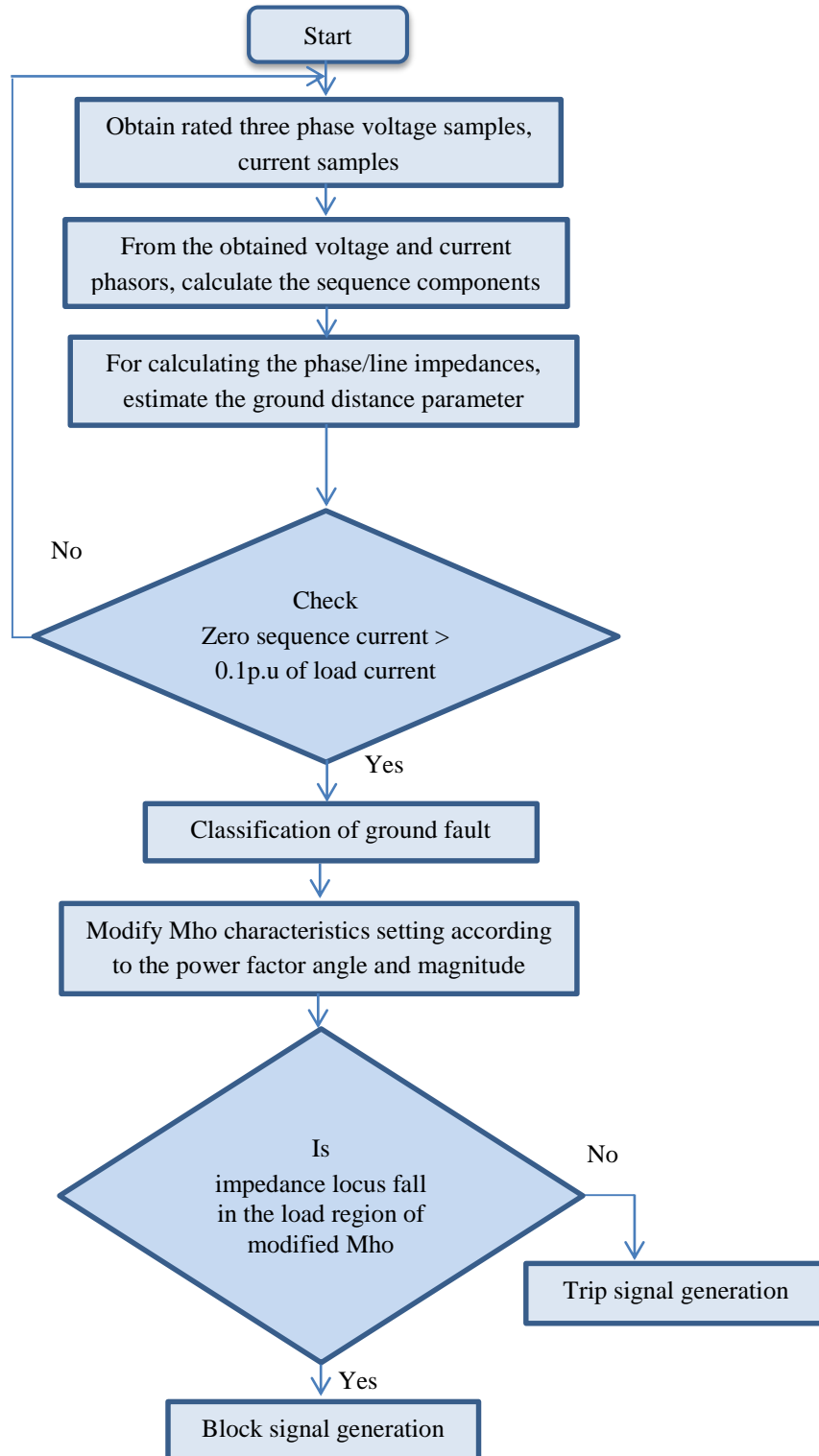
Fig. 1 Proposed methodology

The results exhibit enhanced performance, reducing maloperations during load encroachment while maintaining reliable fault detection capabilities. The proposed scheme addresses the challenges associated with load encroachment by offering a practical and cost-effective solution, contributing to power systems' overall stability and reliability. The scheme enhances operational efficiency and reliability in power transmission networks by preventing

maloperations and accurate fault detection. The structure of the paper is as follows:

Section 2 explains the proposed methodology. Section 3 offers a brief description of the considered system settings. Section 4 discusses the performance evaluation of the proposed method and its comparison with other standard methods. Section 5 focuses on the Experimental results obtained.

2. Proposed Methodology

As previously discussed, the load impedance may temporarily or permanently enter the protection zones in long or heavily loaded power lines. This is a regular occurrence and not a fault. Therefore, the relay should be capable of distinguishing between fault and normal load conditions and refrain from generating any trip command during load encroachment. To achieve this, a scheme has been developed that correctly discriminates between heavy loads and fault scenarios.

Moreover, the zero sequence components of fault currents play a crucial role in distinguishing between High Impedance Faults (HIF) and loads. From the Table 1, It is worth mentioning that zero sequence components exclusively apply to ground faults. In contrast, positive sequence components are relevant for all faults and load conditions in a balanced system. Hence, the positive-sequence impedance of the load can be used to discriminate between loads and faults. The proposed load encroachment logic employs the computation of the positive-sequence impedance of the load ($Z_{measured}$) as a critical factor in its decision-making process. The signal $Z_{inhibit}$ blocks the positive-sequence impedance from declaring a three-phase load.

Table 1. Availability of sequence components

Sequence Components	Availability	Effect of R_f
Positive	For all faults	Yes
Negative	Only unbalanced faults	No
Zero	Only ground faults	No

The flowchart in Figure 1 represents the proposed algorithm of relay decisions during load encroachment conditions.

The following steps explain the proposed method by the flowchart in Figure 1.

1) Collect voltage and current signals. Calculate the sequence components, ground distance Multiplier, and line impedances.

2) If the zero sequence current is more significant than 0.1 p.u of the load current, then classify it as Ground fault.
3) Modify Mho characteristics according to power factor angle and magnitude. Check if the impedance locus falls in the load region. If yes, send a trip signal to the relay or block the signal to the relay.

The proposed method in this study consists of two criteria, which are as follows:

- Criterion I : The adaptive setting of Mho characteristics is employed to determine the relay decision. This criterion focuses on dynamically adjusting the Mho characteristics to enhance the relay's performance.
- Criterion II : The estimation of impedance reach is carried out using sequence components. This criterion involves determining the impedance reach by analyzing the sequence components, which helps accurately identify fault conditions.

These two criteria form the foundation of the proposed method and play a crucial role in improving the reliability and effectiveness of the relay system.

2.1. Criterion I: Development of Adaptive Mho Relay Settings for Protection Zones

To ensure trip prevention during line loading, the traditional phase and ground distance zone configurations are commonly established at 150% of the emergency line ampere rating, along with a bus voltage of 0.85 per unit and a load angle of 30 degrees. These settings are specifically chosen to maintain stability under high-line loads.

The load encroachment regions, which indicate the areas where load conditions may encroach upon the protection zones, are defined in the impedance space of the R-X plane. If the positive sequence impedance falls within the defined region, the 3-phase distance preservation is disabled.

The user sets the defined region with three impedance circles, each with zone 1, zone 2, and zone 3 impedances as radii, and the radiating lines are at a load angle of 30 degrees to avoid tripping distance protection elements during loading. However, this approach can discontinue loadability and threaten system security when emergency switching operations are performed.

Additionally, the 30-degree load angle corresponds to a power factor of 0.87, but in stressed power systems, the power factor may vary. To address this issue, the proposed algorithm sets the Load Encroachment element at varying load angles, corresponding to power factors ranging from 0.8 to 0.9. This approach enhances the system's loadability and enables it to handle load encroachment conditions more effectively.

The proposed approach entails the measurement of voltage and current on the transmission line that necessitates protection. The impedance at the relay location on the transmission line is computed using these measured values. Suppose the calculated impedance falls within the predefined range. In that case, the load encroachment element is activated, preventing the relay from tripping and indicating the existence of a fault on the transmission line. This approach effectively avoids the unnecessary tripping of distance protection elements during line loading. Section 3 of the discussion elaborates on the specific configuration settings for implementing this approach.

2.2. Criterion II: Utilizing Sequence Component Estimation for Impedance Reach Determination

The sequence components of voltages and currents are determined by applying the following equations to the obtained phasors of bus voltages (Va, Vb, Vc) and line currents (Ia, Ib, Ic) during fault conditions:

$$\begin{bmatrix} V_1 \\ V_2 \\ V_0 \end{bmatrix} = \frac{1}{3} \begin{bmatrix} 1 & a & a^2 \\ 1 & a^2 & a \\ 1 & 1 & 1 \end{bmatrix} \begin{bmatrix} V_a \\ V_b \\ V_c \end{bmatrix}$$

$$\begin{bmatrix} I_1 \\ I_2 \\ I_0 \end{bmatrix} = \frac{1}{3} \begin{bmatrix} 1 & 1 & 1 \\ 1 & a & a^2 \\ 1 & a^2 & a \end{bmatrix} \begin{bmatrix} I_a \\ I_b \\ I_c \end{bmatrix}$$

Where $a = 1 \angle 120^0$. The voltages V_1, V_2, V_0 and currents I_1, I_2, and I_0 represent the corresponding positive, negative, and zero sequence components of fault voltages and fault currents, respectively.

For ground faults, the phase impedances with respect to the ground fault can be calculated using the equation:

$$Z_{measured} = \frac{V^P}{I^P + K_0 I_0}$$

Where V^P= positive sequence voltage and I^P= positive sequence current of the line, I_0= zero sequence current, K_0= compensation factor for the compensation of phase to ground impedances during ground faults. The compensation factor, K_0 is expressed as,

$$K_0 = \frac{Z_0 - Z^P}{3 * Z^P}$$

Where Z^P=positive sequence impedance= $\frac{V^P}{I^P}$ and Z_0= zero sequence impedance = $\frac{V_0}{I_0}$. In conventional relay, K_0 is assumed as a constant value between 1.5 and 3.5; instead of considering the compensation factor as a constant value, it can be calculated using various methods, considering factors such as fault resistance, tower footing resistance, and soil resistivity. The specific calculation method may vary depending on the requirements and available data.

Five different compensation factor calculation methods are compared and presented in [33]. In the proposed method, the multiplier $K_{.M.}$ is introduced is used to compensate for the phase-to-ground impedances,

$$K_M = 1 + K_0$$

When an increased resistance ground issue arises, the Zmeasured failure impedance trajectory can lie outside the distance relay's tripping region. This can result in delayed or inadequate tripping, which can be problematic for protective purposes. To address this issue, modifications are made to the relay's characteristics by introducing a compensation multiplier. By incorporating this compensation multiplier, the relay's zone settings are adjusted, providing an extended reach and improving the coverage of faults outside the designated zones. To prevent load encroachment problems, the zero sequence components of fault currents are employed. During load encroachment conditions, the zero sequence components of fault current are constrained within 0.1 per unit of the maximum load currents. This restriction effectively blocks the trip signal to be sent to the circuit breaker, ensuring that the relay does not unnecessarily operate during load-related scenarios.

Furthermore, the proposed algorithm can detect High Impedance Faults (HIF) by monitoring the zero sequence current I0. When the magnitude of the zero sequence current exceeds 0.1 per unit of the maximum load current, it indicates the presence of a high impedance fault. The impedance reach is calculated based on the estimated sequence components and the compensated function incorporating the multiplier. Even if the impedance locus falls within the mho characteristics during high impedance faults, the proposed algorithm can still accurately discriminate between fault and non-fault conditions, showcasing its stability and reliability. For phase faults: The line impedances about phase faults can be calculated using the equation:

$$Z_{ab} = \frac{V_a - V_b}{I_a - I_b} \; ; Z_{bc} = \frac{V_b - V_c}{I_b - I_c} \; ; Z_{ca} = \frac{V_c - V_a}{I_c - I_a}$$

A trip signal is generated when the phase impedances or line impedances complex phasors fall within the mho characteristics. The following section provides a detailed explanation of the proposed algorithm to demonstrate its effectiveness and efficiency.

3. System Study

The diagram in Figure 2 illustrates a double-fed transmission line with inputs at both ends. The system includes two 50 Hz generators, G1 and G2, which provide

three-phase power and a 230 kV transmission line model. The transmission line is divided into two sections, each 120 kilometres long. The positive sequence impedance of the line is 0.287 ohms at an angle of 86.010 degrees, while the zero sequence impedance is 0.844 ohms at an angle of 82.7520

degrees. The nominal voltage is assumed to be 230 kV, and the base power is 100 MVA. A balanced three-phase load rated at 2500 kW is connected to buses B2 and B3 to evaluate the proposed method's effectiveness under fault and load encroachment situations.
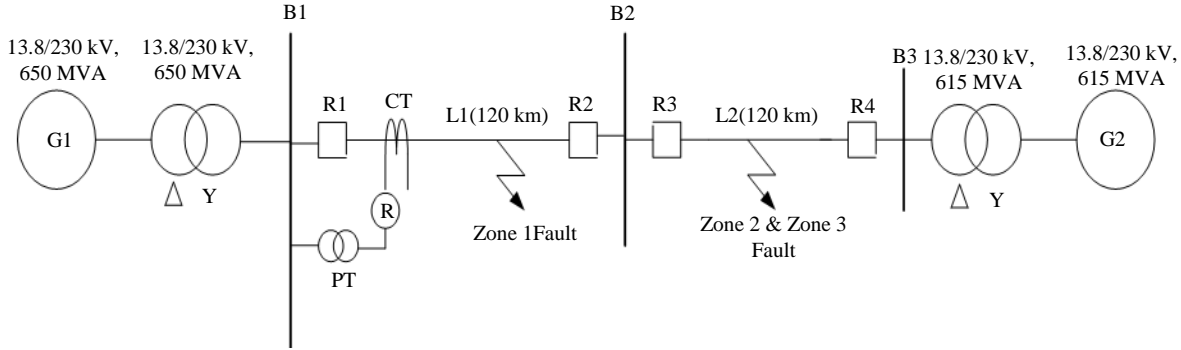
Fig. 2 System modelling

Distance relays typically use three zones of protection: zone-1, zone-2, and zone-3. Zone-1's boundary is set to cover 80% of the total length of the line, and it performs even without scheduled time delay.

The zone-2 element's reach is configured to safeguard the entire transmission line as well as the nearby most minor transmission line, and it performs with an intentional set delay time of 20-30 cycles. Likewise, zone-3 operates with an intentional set delay of 75-90 cycles and includes the total length of the transmission line zone 1 plus 50% of the length of L2 or L3. In the considered system, the Mho impedance zone settings are zone 1, $Z_1=22.96\angle 86.01°$ (80% of line), zone 2, $Z_2=34.44 \angle 86.01°$ (120% of line) and zone $3=Z_3=41.328\angle 86.01°$ (150% with total length of adjacent line).

3.1. Enhanced Mho Relay Settings for Load Encroachment Mitigation

In order to evaluate the methodology's performance, simulations are performed for various fault and load conditions. Based on the detailed discussion in Section 2, traditional methods to prevent load encroachment in distance

relays involve altering the shape of the relay's characteristics. Figure 3 illustrates a mho characteristic diagram of a distance relay in the R-X plane and a load pattern. The shaded area represents the region susceptible to load encroachment. To counter this, additional elements, such as the parallel blinder elements, may be incorporated to truncate a significant portion of the relay's reach characteristics. Another modification involves using smaller, somewhat extended circles, such as ellipses.The conventional methods discussed above have a drawback: they significantly lose the original Mho characteristics coverage. This leads to the possibility of some fault conditions being left undetected by the relay. However, this coverage loss can be avoided using specially configured modified Mho characteristics.

The proposed methodology is shown in Figure 4 and involves a three-zone coverage characteristic comprising zone 1, zone 2, and zone 3 Mho circles. Although three-zone coverage is commonly used in practical protection schemes, the proposed methodology can be modified with different numbers of zones and load patterns based on specific requirements.
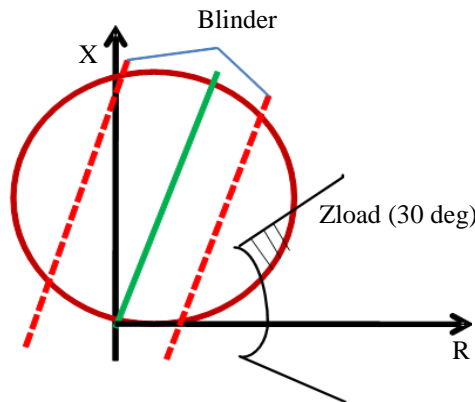
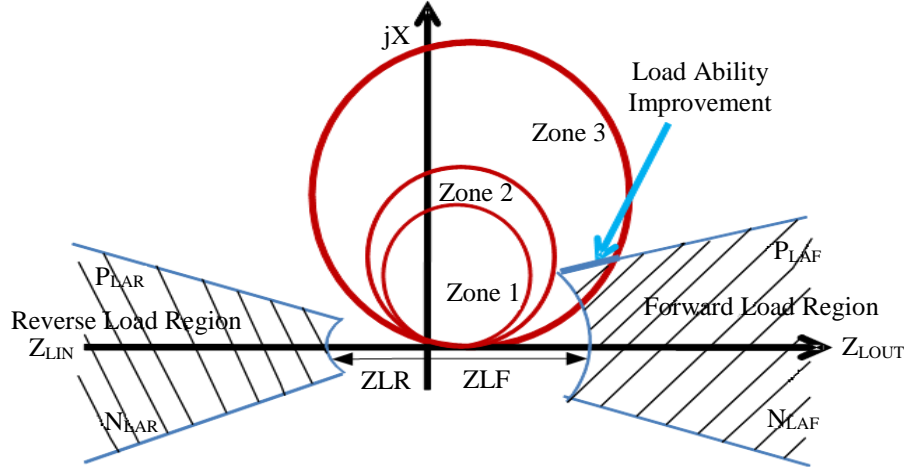

Fig. 3 Conventional mho characteristics

Fig. 4 Modified mho characteristics

The proposed method results in a more minor loss of coverage area than conventional methods. This is achieved by blocking the relay's operation only when its characteristic falls within the load region rather than modifying the existing characteristic to avoid it. The positive sequence complex impedance, Zmeasured, is calculated at the relay location to implement the proposed method. Since the load is generally balanced, the positive sequence impedance provides an accurate measurement. If the locus of $Z_{measured}$ falls within the load region, it indicates a load encroachment condition.

The load region settings are derived as follows. As seen in Figure 3, the magnitude of the load impedance sets the inner boundary of the load region. The upper and lower boundaries of the load region, which extend radially outward from the inner boundary, are determined by the phase angle of the load impedance.

The forward load region Z_{LOUT} is shaded, and the Reverse load region Z_{LIN} is also shaded. In this scenario, the Forward load region Z_{LOUT} encroaches upon zone 3 while Z_{LIN} does not encroach upon any zones.

The inner load region is characterized by magnitude lines, with ZLF representing the Minimum Forward Load Impedance, which corresponds to the maximum load flowing out, and ZLR representing the Minimum Reverse Load Impedance, which corresponds to the maximum load flowing in. These magnitude lines define the boundaries of the inner load region.

The Z_{LIN} and Z_{LOUT} impedances are computed based on the line-to-neutral voltage and line current using the following equations: As the first step to calculate the secondary values, converting Maximum Loads to Equivalent Secondary Impedances.

700 MVA*(1/3) = 233 MVA per phase

230 kV* (1/√3)   = 132.8 kV line-to-neutral

233MVA*(1/132.8 kV)*(1000kV/MV) = 1757A primary

1757A primary*(1/CT ratio)   = 1757 A primary *(1A

                                        secondary /400A primary)

                                        = 4.392 A secondary

132.8 kV * (1000 V/kV)   = 132800 V primary

132800 V primary *(1/PT ratio)   = 132800 V primary

(1 V Secondary /2000 V Primary)   = 66.4 V secondary

For the maximum forward load,

ZLF = 15.11 Ω secondary * 0.9 = 13.60 Ω secondary

$$\frac{230^2 * 400}{800 * 2000} = 13.2 \ \Omega \ secondary$$

For the maximum reverse load,

ZLR= 26.45 Ω secondary * 0.9 = 23.81 Ω secondary

$$\frac{230^2 * 400}{500 * 2000} = 21.1 \ \Omega \ secondary$$

To establish the settings for the radiating lines above and below the Resistance axis in the R.X. plane diagram shown in Figure 3, the load angles P_{LAF} (Maximum Positive Forward Load Angle), N_{LAF} (Maximum Negative Forward Load Angle), P_{LAR} (Maximum Positive Reverse Load Angle), and N_{LAR} (Maximum Negative Reverse Load Angle) must be determined.

The proposed methodology considers a range of power factors for the forward load, from 0.90 lagging to 0.95 leading. Similarly, for the reverse load, the range of power factors extends from 0.80 lagging to 0.95 leading.

The power factor (forward load) can vary from 0.90 lag to 0.95 lead.

Setting $P_{LAF} = \cos^{-1}(0.90) = 26°$

Setting $N_{LAF} = \cos^{-1}(0.95) = -18°$

The power factor (reverse load) can vary from 0.80 lag to 0.95 lead.

Setting $P_{LAR} = 180° - \cos^{-1}(0.95) = 180° - 18° = 162°$

Setting $N_{LAR} = 180° + \cos^{-1}(0.80) = 180° + 37° = 217°$

The power factor of a power signal of the transmission line is the cosine value of the angle between the voltage and the signal's current. The load angles between the voltage and the current signal are calculated from the known power factor of the signal. The angles are obtained by the cosine inverse of the power factor signal of the transmission line.

Hence, from the calculations, we arrive at the values of the magnitude Z_{LF} and Z_{LR} of the line as 13.6 Ω and 23.81 Ω, respectively, while the power factor lines are at and -18° (angles P_{LAF} and N_{LAF}), and (angles P_{LAR} and N_{LAR}) respectively as shown in Figure 5. The obtained impedance trajectory will be compared with a boundary load pattern (shaded area).

If the impedance's magnitude and angle lie within the shaded load pattern, the $Z_{inhibit}$ signal blocks the distance relay elements associated with that particular current phase. As a result, no trip signal is sent to the circuit breaker. A comprehensive explanation of the relay operation logic is provided in the subsequent section for further clarity.

3.2. Operation of Protective Zones in the Relay

The relay operation is governed by the load encroachment logic depicted in Figure 6. The relay signal $Z_{inhibit}$ is utilized to prevent the relay from operating. The region where the load flows out, the Forward load, is represented by the shaded Z_{LOUT} area.
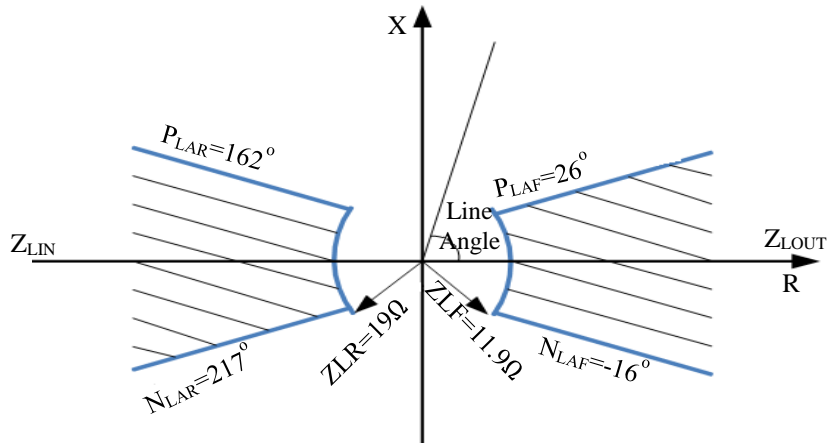

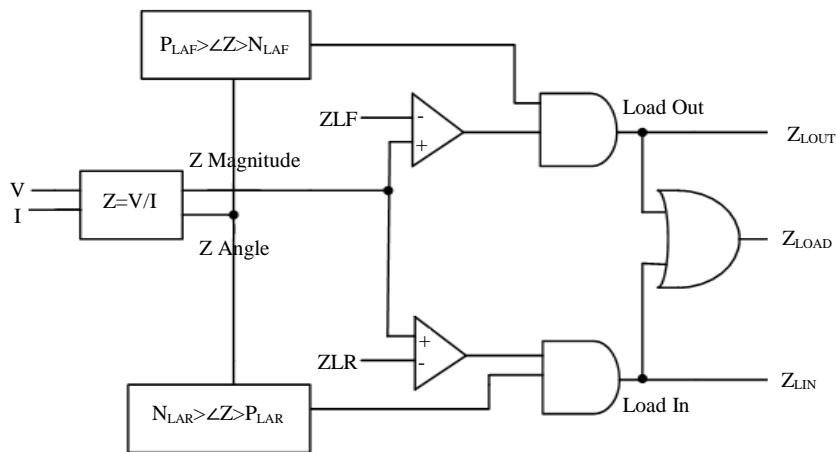**Fig. 5 Load encroachment function settings**

Fig. 6 Load encroachment logic

When the load falls within this forward load region, the signal Z_{LOUT} is set to logical 1. Conversely, the region where the load flows in, referred to as the Reverse load, is depicted by the shaded area labelled as Z_{LIN}. The signal Z_{LIN} is set to logical 1 when the load falls within this reverse load region.

$$Z_{inhibit} = Z_{LOUT} + Z_{LIN}$$

In load conditions, the actual positive sequence impedance can fall within the forward load region, leading to the calculation of $Z_{inhibit}$ as $Z_{LOUT} + Z_{LIN}$, which equals logical $1 + Z_{LIN}$, ultimately resulting in a logical 1 value for $Z_{inhibit}$.

Alternatively, in some cases, the actual positive sequence impedance may fall within the reverse load region, leading to the calculation of $Z_{inhibit}$ as $Z_{LOUT} + Z_{LIN}$, which simplifies to $Z_{LOUT} +$ logical 1, resulting in a logical 1 value for $Z_{inhibit}$. When the system experiences a fault condition, the apparent positive sequence impedance does not fall within either the forward or reverse load region. In this case, the $Z_{inhibit}$ signal is calculated as $Z_{LOUT} + Z_{LIN}$, simplifying to logical 0 + logical 0, resulting in a logical 0 value for $Z_{inhibit}$. This logical 0 value indicates that it is a fault condition and no blocking signal is sent to the circuit breaker, allowing the protective devices to operate and isolate the fault.

A compensation technique involving a Ground Distance Multiplier is employed to mitigate the challenges of high-resistance ground faults. This compensates for the phase-to-ground impedance and extends the reach of the relay's zones. Modifying the relay settings using the ground distance multiplier ensures that the trajectories of high resistance faults fall within the tripping region, preventing delayed tripping or under-reach operation of the relay.

In addition, during load encroachment conditions, the zero sequence components of fault currents are compared to 0.1 per unit (p.u.) of the maximum load current. If the zero sequence components are below this threshold, indicating a load condition, the relay is programmed not to generate a trip signal.

However, with the proposed algorithm, even if the impedance locus falls within the Mho characteristics during load encroachment, a blocking signal is generated to prevent the trip signal from being issued. This enhances the reliability of the protective method by ensuring that load conditions do not trigger unnecessary tripping actions.

4. Performance Evaluation of the Proposed Algorithm

Different faults and load conditions are simulated for the validation of the proposed methodology, and the results are obtained for various power system operating conditions.

4.1. Case 1: During Phase to Neutral Fault Condition

The proposed algorithm utilizes impedance thresholds set for different zones to determine whether the relay should trip. The calculated impedance is compared against these thresholds to make the decision.

The fault current's zero sequence component is considered to determine the line's impedance locus. Under normal conditions, the zero sequence component is negligible but rapidly increases when a ground fault occurs. This algorithm assumes a threshold value of 0.1 per unit (p.u.) of the maximum load current for the zero sequence current. If the zero sequence current exceeds this threshold, it indicates the occurrence of a fault.

Based on the system study described in Section 2, where the maximum load MVA rating is 700 MVA and the nominal secondary current derived is 4.392 A, the proposed algorithm sets a minimum threshold value of 0.1 p.u. for the zero sequence current to enable the operation of the distance relay's ground unit. This threshold value is three times the zero sequence current threshold: $3I0$ threshold $= 0.1 * 4.392 = 0.4392$ A (minimum zero sequence current to allow operation of the distance relay ground unit).

To illustrate the algorithm's operation, an A.G. fault is simulated in the system between phase A and ground, located 5 km from bus B1, with a fault resistance of 10 Ω. The fault current and voltage values measured during the fault condition at Relay R1 are presented in Table 2.

Table 2. Fault current and voltage data at relay R_1 during A.G. fault

Currents	Voltages
$I_a = 0.68\angle -150.23°$	$V_a = 10.46\angle -64.84°$ V
$I_b = 0.13\angle 81.32°$ A	$V_b = 114.97\angle 139.05°$ V
$I_c = 0.12\angle 171.63°$ A	$V_c = 120.49\angle 28.19°$ V

The compensation factor K_0 is calculated for the phase A to ground fault scenario and incorporated into the measured impedance calculation to obtain the compensated impedance. The sequence components are then calculated using the following formula:

$$\begin{bmatrix} I_1 \\ I_2 \\ I_0 \end{bmatrix} = \frac{1}{3} \begin{bmatrix} 1 & 1 & 1 \\ 1 & a & a^2 \\ 1 & a^2 & a \end{bmatrix} \begin{bmatrix} I_a \\ I_b \\ I_c \end{bmatrix}$$

$$3I_0 = 0.72 \angle 164.60^0$$

Based on the detection of a ground fault, the actual zero sequence component of the current exceeds the threshold value, indicating the presence of a fault. To calculate the measured impedance, the compensation factor is determined. The compensation factor K_0 is calculated as,

$$K_0 = \frac{Z_0 - Z^P}{3 * Z^P} = \frac{0.1065 + j0.83 - (0.02 + j0.287)}{3 * (0.02 + j0.287)}$$

$$= 0.65 \angle -9.95 = 0.62 - j0.19$$

Then, as per the proposed algorithm, the Ground Distance Multiplier used to compensate for phase-to-ground impedances is

$$1 + K_0 = 1 + (0.62 - j0.19) = 1.62 - j0.19 = 1.62 \angle 353.31^0$$

The setting calculations for the three zones (zone 1, zone 2, and zone 3) are determined based on the compensated impedance. The specific calculations for each zone setting are as follows:

Compensated ground distance setting (zone 1 phase-to-ground compensated Mho impedance)

$$22.96 \ \Omega \ \angle 86.01^0 * 1.62 \angle 353.31^0 = 37.92 \ \Omega \ \angle 79.32^0$$

Compensated ground distance setting (zone 2 phase-to-ground compensated Mho impedance)

$$34.44 \ \Omega \ \angle 86.01^0 * 1.62 \angle 353.31^0 = 55.79 \ \Omega \ \angle 79.32^0$$

Compensated ground distance setting (zone 3 phase-to-ground compensated Mho impedance)

$$41.33 \ \Omega \ \angle 86.01^0 * 1.62 \angle 353.31^0 = 66.95 \ \Omega \ \angle 79.32^0$$

The measured impedance is calculated as

$$Z_{measured} = \frac{V_a}{I_a + K_0 I_{a0}}$$

$$= \frac{10.46 \angle -64.84^0}{0.68 \angle -150.23^0 + 1.62 \angle 353.31^0 * 0.24 \angle 164.60^0}$$

$$= 5.209 \ \angle -25.19^0$$

The measured impedance is lesser than the zone 1 set impedance; the fault occurs in zone 1. During the occurrence of a fault, power flow is typically transferred in the direction of the fault. In this case, with a phase-to-phase fault between phase B and phase C, the power flow will be transferred in the forward direction of the relay, following the fault path.

4.2. Case 2: During Load Condition
Table 3 presents the performance of the proposed method under diverse load and fault scenarios. The input parameters for load encroachment condition, namely Z_{LF}=11.9 Ω, Z_{LR}=19 Ω, P_{LAF}=260, N_{LAF}=3420, P_{LAR}=1620, and N_{LAR}=2170 are set in the EMTP software.

The power system load is above its rated value to create various load and fault simulation scenarios, tabulated in Table 3 for analysis and evaluation.

Table 3. Proposed algorithm response to load conditions

Case No.	Load at Bus 1	Loading of Line 1-2 (% of Rated Load)	Zone R1		LE	Disturbance Detected	Decision Taken			
			Measured Impedance	Response			PM	AB [18]	WB [21]	FB [22]
1	2000	96	X	X	X	Fault	No	Yes	Yes	Yes
2	2500	116	X	X	X	Fault	No	Yes	Yes	Yes
3	2750	130	$35.73 \angle 0.52^0 \Omega$	Zone-3	Z_{LOUT}	LE	Yes	Yes	Yes	Yes
4	3750	137	$37.34 \angle 72.37^0 \Omega$	Zone-3	Z_{LIN}	LE	Yes	Yes	Yes	Yes
5	4000	142	$40.54 \angle 83.45^0 \Omega$	Zone-3	Z_{LOUT}	LE	Yes	Yes	Yes	Yes

LE-Load Enchroachment; PM-Proposed Method; AB-Admittance-Based algorithm; WB-Fast Wavelet-Based method; FB-Frequency Based method

The load encroachment condition is created by increasing the load of buses B_1 and B_2 above its rated load of 2000W. Till the load is 2500W, the load encroachment condition is not created, but when the load is increased more than 2500W, the impedance trajectory enters the load region Z_{LOUT}.

The third case in Table 3 considers a scenario where a load of 2750 W is connected to bus B1. The load current flows out of the bus and falls within the shaded region Z_{LOUT},

representing the forward load. As a result, the apparent positive-sequence impedance falls within the Z_{LOUT} area, leading to the following outcomes.

$$Z_{inhibit} = Z_{LOUT} + Z_{LIN} = logic \ 1 + Z_{LIN} = logic \ 1$$

The Relay Word bit $Z_{inhibit}$ asserts to logical 1. The logic sends a blocking signal to the relay R_1 because the $Z_{inhibit}$ asserts logical 1, so the breaker is not activated. Figure 7 shows the breaker signal BRK is not asserting during this

forward load conditions. The operation of relay R_1 is blocked and alerts the operator about the situation. Case 4 of Table 3 is discussed as a load of 3750 W is applied at bus B_1, and this case shows the load output in the reverse direction. The load impedance enters the Z_{LIN} area since the phase angle of the load current angle is 90^0 to 270^0. The load flowing IN lies within the hatched region Z_{LIN}, representing reverse load. The apparent positive-sequence impedance is within the Z_{LIN} area, resulting in the following.

$$Z_{inhibit} = Z_{LOUT} + Z_{LIN} = Z_{LOUT} + logic\ 1 = logic\ 1$$

The relay word bit $Z_{inhibit}$ asserts to logical 1. The logic sends a block signal to the relay R_1 when the $Z_{inhibit}$ bit asserts logical 1. The operation of relay R_1 is blocked and alerts the operator about the situation. Figure 8 shows the breaker signal BRK is not asserting during this reverse load condition.
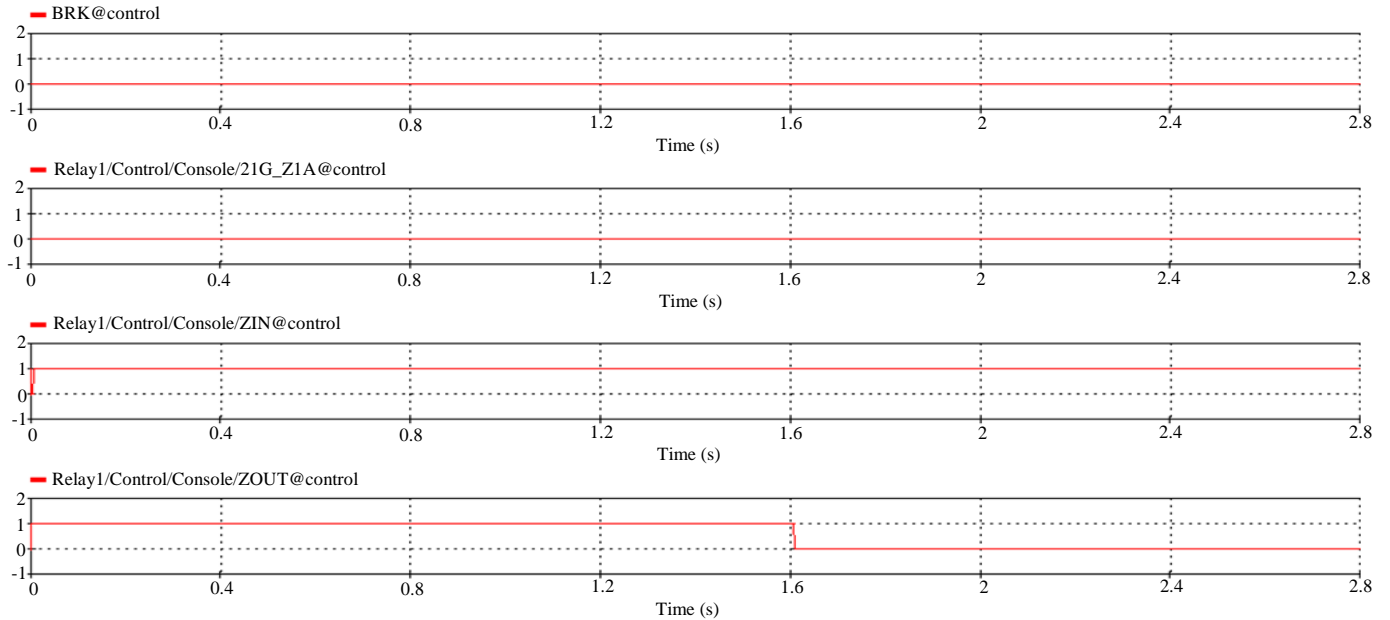
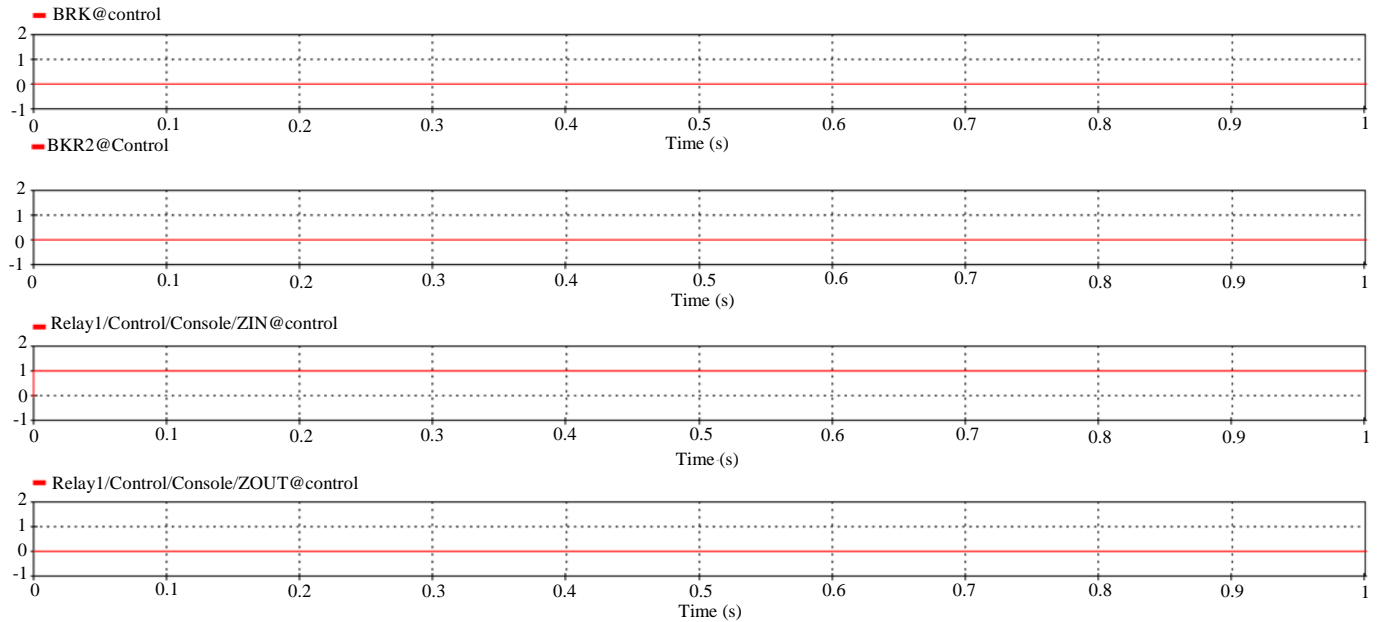

Fig. 7 Signals during forward load conditions

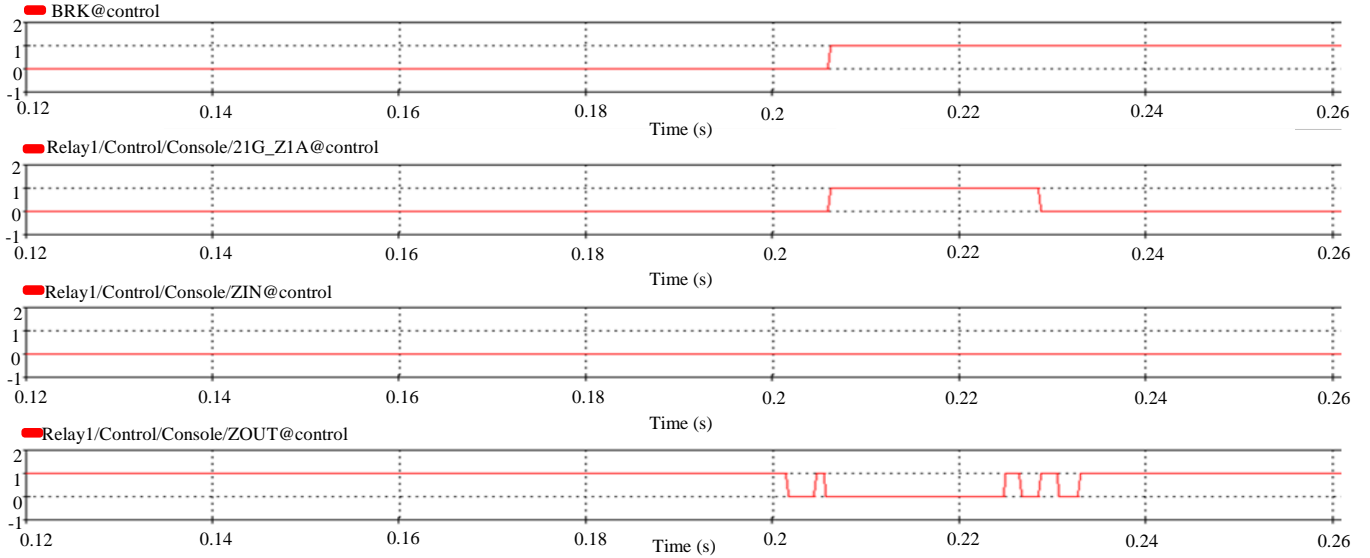**Fig. 8 Signals during reverse load conditions**

Fig. 9 Signals of fault during load conditions

During load encroachment conditions, faults may also occur in the power system. In order to obtain the performance of the system during that condition, a fault is simulated during load encroachment conditions. The breaker BRK starts its operation at 222 ms when the A.G. fault occurs at 200 ms even though load encroachment condition exists, showing signals in Z_{IN} and Z_{OUT} regions as shown in Figure 9. A fault is preferred even when the breaker is blocked during load encroachment conditions.

4.3. Case 3: During Phase-to-Phase Fault Condition
A phase-to-phase fault is simulated between phases B and C, located 90 km from bus B_1. During this fault condition, the fault currents and voltages at Relay R1 are measured and recorded for analysis. We calculate the threshold current from the obtained phase current during phase fault. The threshold current setting is calculated as follows.

Delta Current = 3.0 A (minimum phasor difference between any two phases). The minimum threshold current required is calculated by adding 5% to ensure the threshold value's certainty: 3.0*105 percent = 3.2A.

Since B phase = C phase, actual minimum threshold current = (3.2/2) = 1.6 A. If any phase currents exceed the threshold current, the phase distance element will detect the presence of a phase fault and initiate its operation. The fault current and voltage data collected at Relay R1 during this fault condition are recorded and presented in Table 4.

Based on the results obtained, it is observed that the phase current exceeds the minimum threshold current, and the current at the B-phase has an opposite polarity compared to the current at the C-phase. Consequently, the B-phase and C-phase currents magnitudes are equal but 180 degrees out of phase. The ground distance element identifies this situation as a two-phase fault between phase B and phase C, triggering the activation of the two-phase tripping element in relay R_1. The calculated actual impedance in this scenario is determined.

$$Z_{measured} = \frac{V_b - V_c}{I_b - I_c}$$

$$= \frac{37.4 \angle -152.50^0 - (37.5 \angle 152.5^0)}{2.25 \angle 170^0 - (2.25 \angle 170^0)}$$

$$= 4.912 \angle -0.113 \ \Omega$$

The measured impedance is lesser than the zone 1 set impedance, and the fault occurs in zone 1, the impedance locus enters zone 1 Mho Characteristics.

Table 4. Fault current and voltage data at relay R_1 during phase fault condition

Currents	Voltages
Ia=0.76∠ -90º A	Va=66.4∠ -0º V
Ib=2.23∠-170º A	Vb=37.4∠ -152.50º V
Ic=2.25∠ 170º A	Vc=37.5∠ 152.5º V

4.4. Case 4: During Three-Phase Fault Condition
A simulated three-phase fault is initiated 90 km from bus B_1 in the power system model. We calculate the threshold current from the obtained phase current during the fault. The threshold current setting is calculated as follows

Delta Current = 3.0 A (minimum phasor difference between any two phases). The minimum threshold current required is calculated by adding 5% to ensure the threshold value's certainty: 3.0*105 percent = 3.2A.

Since A Phase = B phase = C phase, actual minimum threshold current = (3.2/3) = 1.07 A. If any phase current exceeds the threshold current, the phase distance element will detect the phase fault and operate. The fault current and voltage data obtained at Relay R_1 are tabulated in Table 5.

Table 5. Fault current and voltage data at relay during three phase fault condition

Currents	Voltages
I_a=0.79∠ -151.73^o A	V_a=6.79∠ -65.81^o V
I_b=0.79∠ 88.26^o A	V_b=6.79∠ 174.18^o V
I_c=0.79∠ -31.74^o A	V_c=6.79∠ 54.19^o V

The actual impedance is calculated as

$$Z_{measured} = \frac{V_a}{I_a}$$

$$= \frac{6.79∠ - 65.81^0}{0.79∠ - 151.73^0} = 0.6148 + j8.6 \ \Omega$$

Zone 1 fault is confirmed as the measured impedance is lower than the zone 1 set impedance. The effectiveness of the proposed technique is demonstrated by comparing its results with previous methods using similar system configurations, which is explained in the subsequent section.

4.5. Validation of the Proposed Method
As detailed in Section 2, the proposed relaying technique was validated, and its effectiveness and settings were verified through simulations of various fault scenarios under different power system conditions.

The simulation results are presented in Tables 6, 7, and 8, which respectively showcase the operating time of the proposed numerical technique for close-in, boundary, and high resistance faults. Additionally, Table 9 presents the results of the proposed numerical algorithm under load encroachment conditions. To evaluate the performance of the proposed method, the achieved results were compared with existing methods such as the admittance-based algorithm [18], Fast wavelet-based method [21], and frequency-based method [22]. These comparisons allow for assessing the proposed technique's superiority in terms of operating time and reliability in various fault scenarios.

Table 6. Proposed algorithm response for close in faults

Case No.	Fault Type	Rf	Location	Operating Time (ms)			
				Proposed Method	AB [18]	WB [21]	FB [22]
1	A-G	0.01	5	5.2	5.30	5.6	13
2	A-G	10	5	4.5	4.52	7.6	14
3	A-G	20	5	3.9	4.21	3.2	18
4	A-G	0.01	10	5.41	5.51	5.6	8
5	B-G	10	10	4.7	4.83	7.6	16
6	C-G	20	10	4.4	4.49	3.2	18
7	ABG	0.01	5	4.3	4.30	5.4	12
8	ABG	10	5	4.32	4.61	7.3	13
9	ABG	20	5	4.45	5.10	3.3	15
10	ACG	0.01	10	4.15	4.20	-	-
11	ACG	10	10	4.5	4.85	-	-
12	ACG	20	10	5.10	5.30	NOP	NOP
13	ABCG	0.01	5	5.50	5.81	NOP	8

Table 7. Proposed algorithm response for boundary faults

Case No.	Fault Type	Rf	Location	Operating Time (ms)			
				Proposed Method	AB [18]	WB [21]	FB [22]
14	A-G	0.01	30	5.9	6.2	12.4	9
15	C-G	20	30	10.8	11.5	13.0	18
16	A-G	40	30	10.9	11.9	14.4	20
17	ABG	0.01	30	3.9	4.12	-	10
18	A-G	0.01	50	11.5	12.5	11.6	15
19	B-G	20	50	11.6	12.6	15.2	18
20	C-G	40	50	12.8	13.9	18.0	20
21	BCG	0.01	50	8.5	9.00	-	11
22	AG	0.01	65	13.5	14.3	16.4	16
23	AG	20	65	14.6	15.5	22.0	18
24	AG	50	65	14.9	15.8	NOP	19
25	ABG	0.01	65	8.9	11.2	-	12
26	ABCG	0.01	65	9.5	10.0	-	10
27	AG	0.01	90	16.8	17.3	23.0	17
28	AG	20	90	17.3	18.5	26.0	18
29	AG	50	99	18.6	19.6	NOP	NOP
30	CAG	0.01	99	12.9	13.10	-	13

Table 8. Proposed algorithm response for different faults

Case No.	Fault Type	Rf	Location	Operating Time (ms)			
				Proposed Method	AB [18]	WB [21]	FB [22]
31	AG	0.01	110	212.3	225.5	NOP	NOP
32	BG	0.01	150	214.5	227.3	NOP	NOP
33	CG	20	150	218.5	229.2	NOP	NOP
34	AG	20	180	410.6	735.2	NOP	NOP
35	BG	50	180	410.6	742.2	NOP	NOP

AB-Admittance-Based algorithm; WB-Fast Wavelet-Based method; FB-Frequency Based method; NOP-No Operation

Table 9. Proposed algorithm response for load conditions

S. No.	Load at Bus 1	Loading of Lines 1-2 (% of Rated load)	Zone R1		LE	Disturbance Detected	Decision taken			
			Measured Impedance	Response			PM	AB [18]	WB [21]	FB [22]
1	2000	96	X	X	X	Fault	No	Yes	Yes	Yes
2	2500	116	X	X	X	Fault	No	Yes	Yes	Yes
3	2750	130	$35.73\angle 0.52^0\Omega$	Zone-3	Z_{LOUT}	LE	Yes	Yes	Yes	Yes
4	3750	137	$37.34\angle 72.37^0\Omega$	Zone-3	Z_{LIN}	LE	Yes	Yes	Yes	Yes
5	4000	142	$40.54\angle 83.45^0\Omega$	Zone-3	Z_{LOUT}	LE	Yes	Yes	Yes	Yes

LE-Load Enchroachment; PM-Proposed Method; AB-Admittance-Based algorithm; WB-Fast Wavelet-Based method; FB-Frequency Based method

Figure 10(a) depicts the impedance locus during a low-resistance close-in L-G fault. In contrast, Figures 10(b) and 10(c) illustrate impedance trajectories for high resistance L-G faults simulated at different locations on the line between B2 and B3. Figure 10(d) showcases the impedance locus during a high resistance L-G fault. It is evident that during high impedance faults, the impedance locus falls outside the mho characteristics of standard relays.

The proposed algorithm addresses this issue by obtaining compensated impedance through the ground distance multiplier. Three-zone coverage characteristics, namely zone 1, zone 2, and zone 3 Mho circles, are established based on the compensated impedance. Figure 9 displays the modified Mho characteristics incorporating the Compensated Fault impedance trajectory.

Figures 11(a), 11(b), 11(c), and 11(d) demonstrate impedance trajectories falling within the compensated zone settings. Notably, the proposed compensated characteristics of the relaying scheme effectively enhance fault coverage and generate a trip signal to activate the circuit breaker during high-impedance faults. This showcases the effectiveness of the proposed methodology.
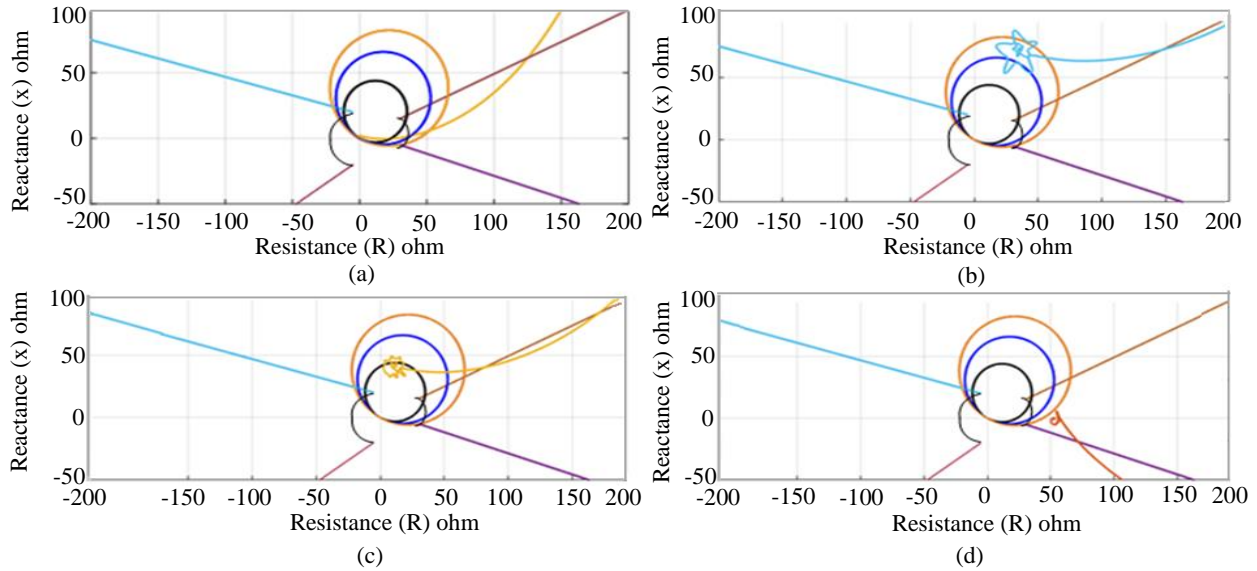

Fig. 10 Impedance trajectory of fault during (a) Case 1 of table 3, (b) Case 27 of table 4, (c) Case 31 of table 5, and (d) Case 36 of table 5.
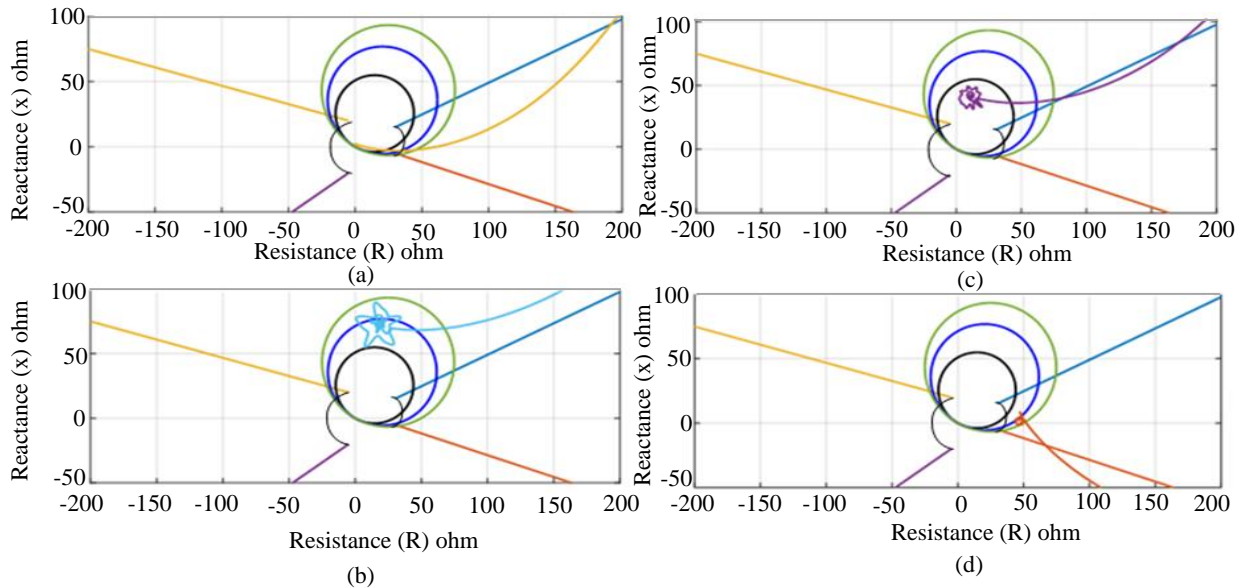

Fig. 11 Compensated impedance trajectory of fault during (a) Case 1 of table 3, (b) Case 27 of table 4, (c) Case 31 of table 5, and (d) Case 34 of table 5.

The proposed method was rigorously tested in a simulated power system network to evaluate its effectiveness in handling various fault scenarios, including L.G., L.L., LLG, and LLLG. The simulations encompassed close-in, boundary, in-zone, and out-of-zone faults, providing comprehensive coverage.

Faults with resistance values ranging from 0.01 to 200 Ω were considered, and the system load was intentionally increased beyond its rated capacity. The distance relay was implemented using MATLAB/SIMULINK, generating numerous simulation cases.

The sequence components were estimated using voltage and current phasors, with specific compensation applied for ground faults. The load region was determined based on positive sequence components, and the proposed methodology successfully distinguished between load encroachment and fault conditions. The adaptive setting of Mho characteristics, which considered a wide range of power angles, proved highly efficient in optimizing the relay's performance. The numerical relay exhibited excellent performance for the protection scheme, with results obtained for different fault and load conditions based on the discussed settings. Figures 12(a), 12(b), 12(c), 12(d), 12(e), 12(f), 12(g), and 12(h) provide visual representations of various fault and load conditions. During a low resistance L-G fault, the assessed impedance locus is shown in Figure 12(a). Figures 12(c) and 12(e) depict a fault between B1 and B2, indicating a zone 1 fault. Figure 12(g) represents a low resistance L-G fault simulated at a location between B2 and B3. Figure 12(f) represents a very high resistance fault.

On the other hand, Figures 12(b), 12(d), and 12(h) illustrate load encroachment conditions. In load conditions, the impedance locus during a fault falls outside the mho characteristics of typical relays but remains within the load region.

The proposed mathematical relaying methodology modifies the Mho characteristics only during a fault and generates a trip signal to activate the circuit breaker. This highlights the effectiveness of the proposed method. The responsive configuration of the mathematical relay proves highly efficient for the protection scheme under consideration.
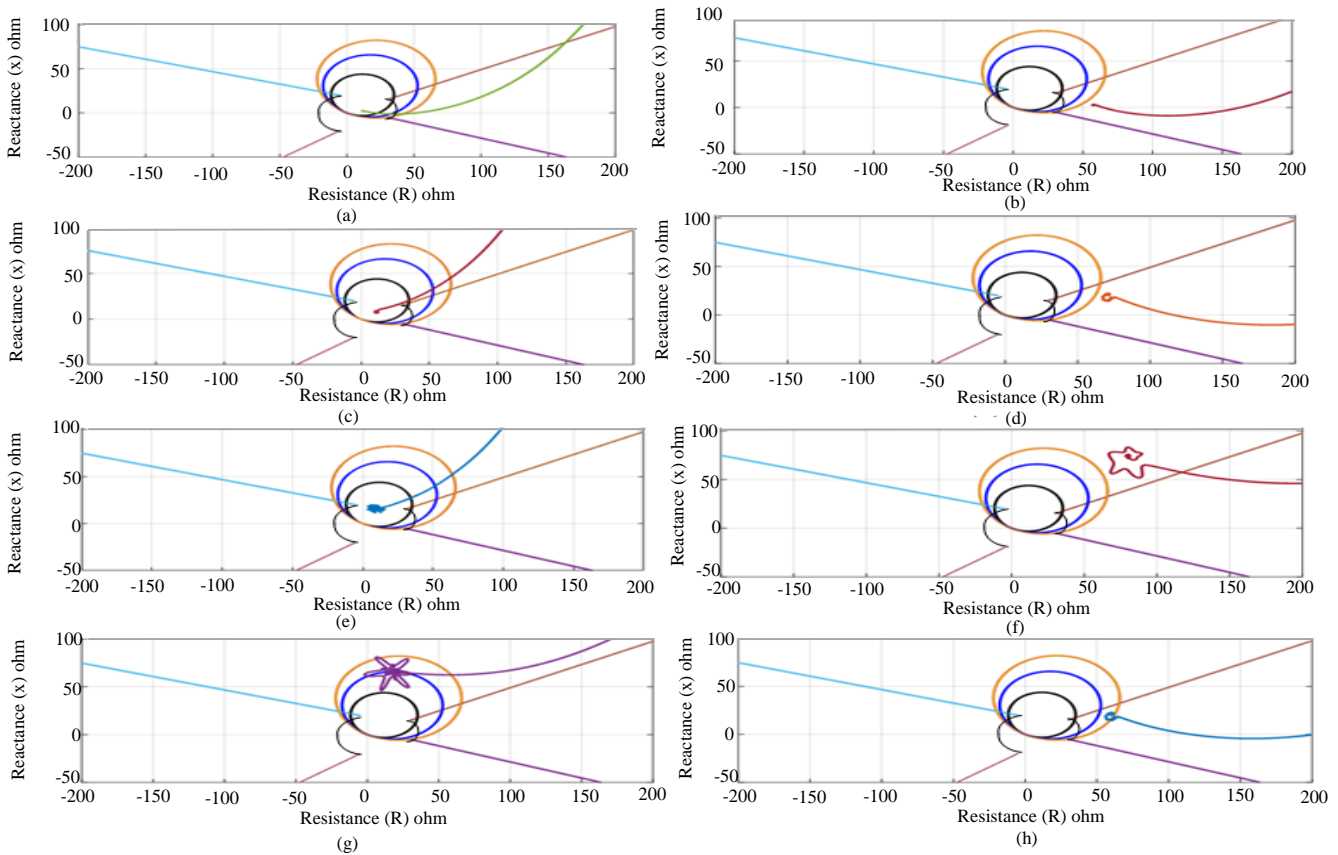

Fig. 12 Fault impedance trajectories during (a) Case 3 of table 3, (b) Case 38 of table 6, (c) Case 14 of table 4, (d) Case 39 of table 6, (e) Case 16 of table 3, (f) Case 35 of table 5, (g) Case 32 of table 5, and (h) Case 40 of table 6.

5. Experimental Results

To verify the working of the proposed method and its strategy, the load encroachment settings are implemented in– a time environment Electromagnetic Magnetic Transient Program–Revised Version (EMTP-RV), and the signals and impedance trajectories of the relays are generated for various cases.

Figure 13(a) shows the impedance trajectory of Relay 1 tripping at zone 2. The locus starts from the origin, picks up at zone 2 and reaches back to the origin. Figure 13(b) shows

the impedance trajectory of relay 2 tripping at zone 1. The locus starts from the origin, picks up at zone 1 and reaches back to the origin. Figure 14 shows the impedance locus in zone 3, but no signal is sent to the breaker. This explains clearly that the tripping signal is not sent to the breaker even if the impedance lies in zone 3 because of the load encroachment.

Figure 15 shows the locus of the impedance when a fault exists during load encroachment conditions. The locus starts from the origin, picks up at zone 3 and reaches back to the origin.
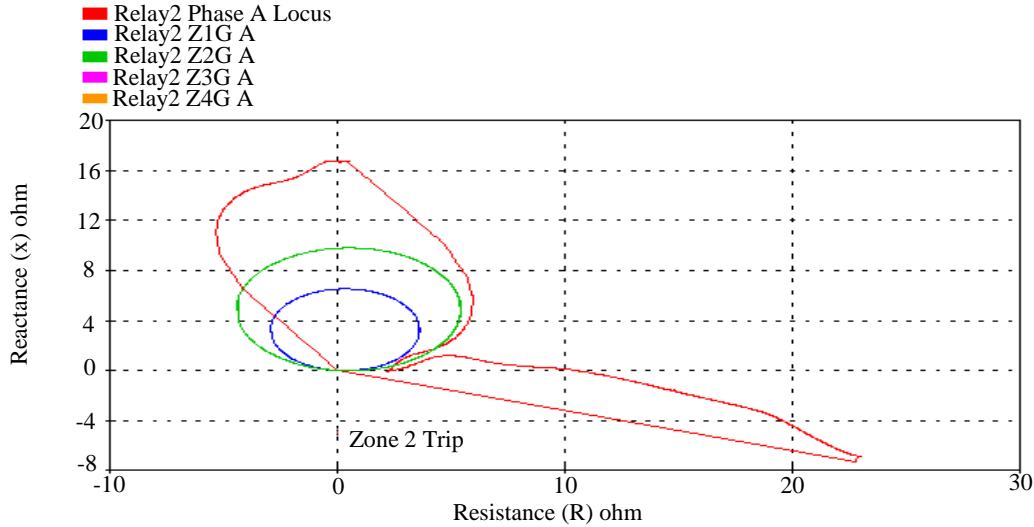

Fig. 13(a) Impedance trajectory of relay 1 tripping at zone 1
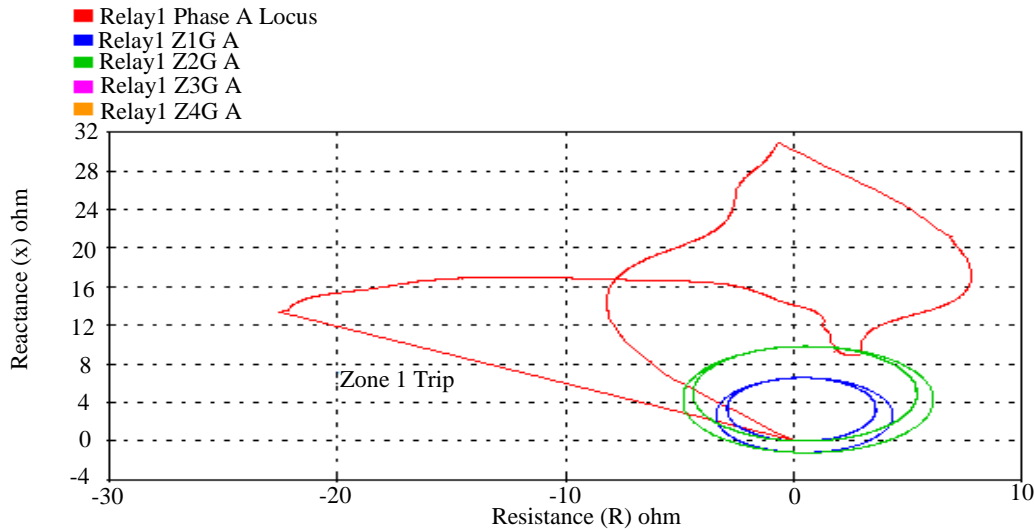

Fig. 13(b) Impedance trajectory of relay 2 tripping at zone 1

The proposed method demonstrates clear advantages over conventional approaches. It excels in speed, particularly for close-in faults, and consistently achieves shorter relay operating times even for low resistance faults. Unlike traditional methods, the proposed approach accurately identifies high resistance faults within their designated zones, enhancing system reliability. It also effectively distinguishes

between fault zones and operates within the allocated time margin. Moreover, the developed methodology exhibits stability even under load encroachment conditions.

Overall, the proposed method offers improved speed, accurate fault identification, optimized zone discrimination, and stability, making it a valuable and reliable solution.
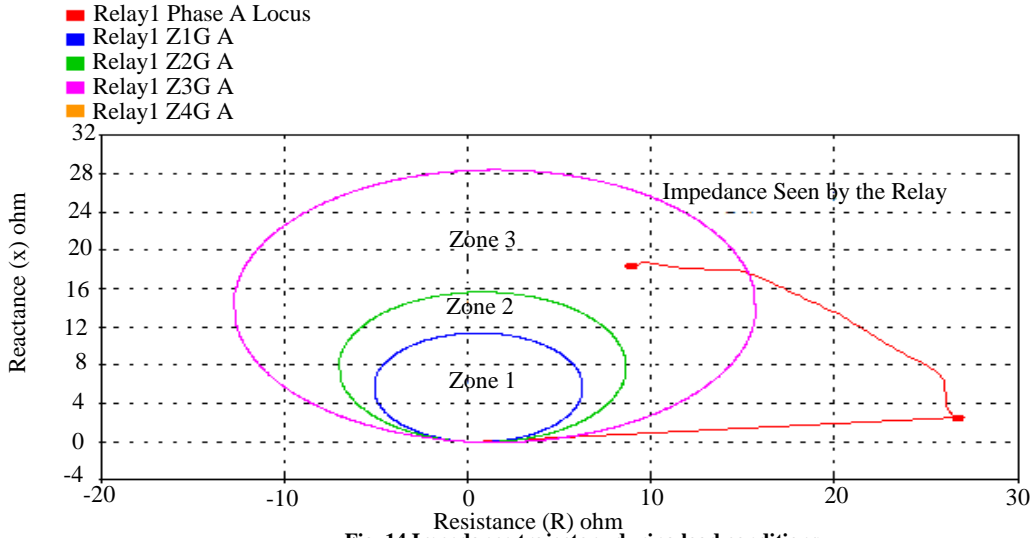
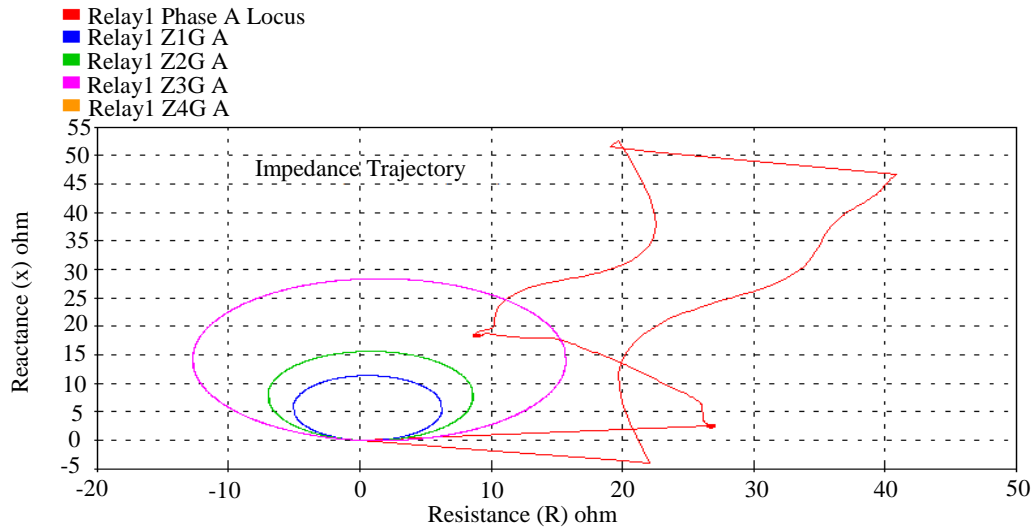**Fig. 14 Impedance trajectory during load conditions**

**Fig. 15 Impedance trajectory of fault during load conditions**

After analyzing the comparison results, several observations can be made. Firstly, the admittance-based method (referenced as [21]) shows a shorter operating time for close-in faults, but its response time decreases as the fault resistance increases.

On the other hand, the wavelet-based method (referenced as [24]) exhibits slightly lower response time than the proposed algorithm for long-distance faults. However, the proposed algorithm demonstrates improved response time for faults with high resistance.

It is worth noting that the proposed methodology incorporates a more extended reach setting of 100 km for zone 1. While this may result in a slower response time for out-of-zone faults, it ultimately showcases the reliability and stability of the proposed methodology. The comparison of the relay response time of various zone faults is obtained for the admittance-based method, and the proposed method is given in Figure 16. These tested waveforms and results prove the method's validity and working, ensuring timely adjustments and preventing false tripping. In conclusion, with its adaptive approach, the implemented methodology delivers the best overall accuracy and response time performance.

It successfully combines the advantages of shorter operating time for close-in faults and improved response time for faults with high resistance, making it a reliable and efficient solution.
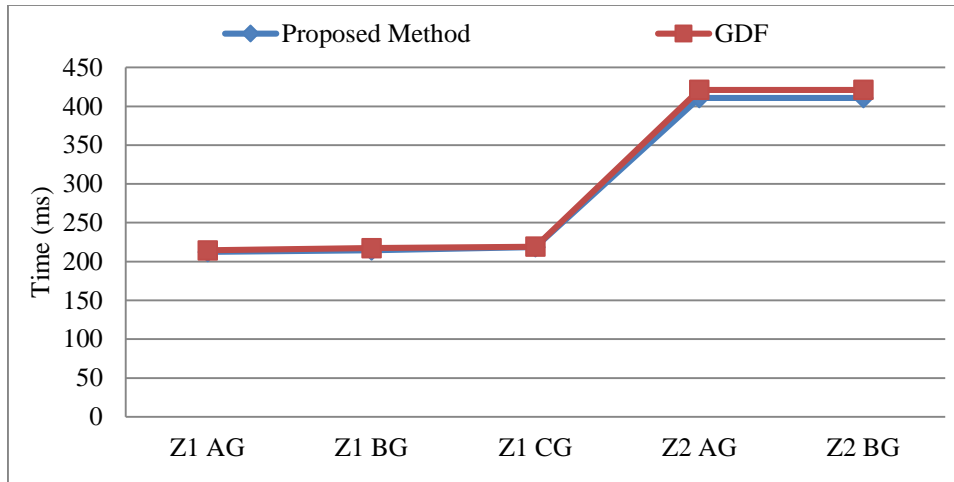
Z1 AG-Zone 1 A.G. Fault, Z1 BG-Zone 1 B.G. Fault, Z1 CG-Zone 1 C.G. Fault, Z2 AG-Zone 2 A.G. Fault, Z2 BG-Zone 2 B.G. Fault
Fig. 16 Relay response time comparison for A.B. method and proposed method

6. Conclusion

This article aims to improve the numerical distance relay impedance range by using an adaptive setting of Mho relay characteristics. The proposed technique employs modified Mho characteristics for a responsive numerical relaying configuration, which is modelled in MATLAB software and validated through simulation for various power system disturbances. The method effectively identifies high-impedance faults by estimating zero sequence components and discriminating between load and fault conditions. The calculation of the ground distance multiplier achieves compensation for adaptive Mho relay characteristics.

Compared to conventional methodologies, the proposed methodology is particular and faster during close-in faults, high resistance faults, and load encroachment conditions. The proposed algorithm significantly improves the sensitivity and stability of distance relays.

References

[1] Vassilis C. Nikolaidis, Aristotelis M. Tsimtsios, and Anastasia S. Safigianni, "Investigating Particularities of Infeed and Fault Resistance Effect on Distance Relays Protecting Radial Distribution Feeders with DG," *IEEE Access*, vol. 6, pp. 11301-11312, 2018. [CrossRef] [Google Scholar] [Publisher Link]

[2] Behrooz Taheri, Seyed Amir Hosseini, and Sirus Salehimehr, "An Overview of Power Swing Detection Methods in Distance Relays and the Factors Involved," *IET Generation, Transmission & Distribution*, vol. 17, no. 4, pp. 743-761, 2023. [CrossRef] [Google Scholar] [Publisher Link]

[3] K.B. Veeresha, M.G. Manjula, and A.H. Thejaswi, "Enhancement of Power Quality Using Single Phase Generalised Unified Power Quality Conditioner in Distribution System," *International Journal of Recent Engineering Science*, vol. 10, no. 4, pp. 1-6, 2023. [Google Scholar] [Publisher Link]

[4] Subhradeep Barman, and Biman Kumar Saha Roy, "Detection and Location of Faults in Large Transmission Networks Using Minimum Number of Phasor Measurement Units," *IET Generation, Transmission & Distribution*, vol. 12, no. 8, pp. 1941-1950, 2018. [CrossRef] [Google Scholar] [Publisher Link]

[5] Sambeet Mishra et al., "A Multi-Agent System Approach for Optimal Microgrid Expansion Planning under Uncertainty," *International Journal of Electrical Power & Energy Systems*, vol. 109, pp. 696-709, 2019. [CrossRef] [Google Scholar] [Publisher Link]

[6] S. Golhani, and S. Bhongade, "Detection and Error Analysis of High Impedance Fault Using Wavelet Transform, Traveling Wave and Support Vector Machine," *IUP Journal of Electrical & Electronics Engineering*, vol. 11, no. 2, pp. 7-13, 2018. [Google Scholar] [Publisher Link]

[7] Niharika Agrawal, and Mamatha Gowda, "Power Flow Enhancement by TCSC Using Two Different Types of Pulse Generators," *International Journal of Recent Engineering Science*, vol. 9, no. 1, pp. 31-38, 2022. [CrossRef] [Google Scholar] [Publisher Link]

[8] Rahman Dashti et al., "A Survey of Fault Prediction and Location Methods in Electrical Energy Distribution Networks," *Measurement*, vol. 184, 2021. [CrossRef] [Google Scholar] [Publisher Link]

[9] B. Suresh Babu, "Real Power Loss Minimization of AC/DC Hybrid Systems with Reactive Power Compensation by Using Self Adaptive Firefly Algorithm," *SSRG International Journal of Industrial Engineering*, vol. 7, no. 1, pp. 41-48, 2020. [CrossRef] [Google Scholar] [Publisher Link]

[10] Mengxiao Chen et al., "Research on a Distance Relay-Based Wide-Area Backup Protection Algorithm for Transmission Lines," *IEEE Transactions on Power Delivery*, vol. 32, no. 1, pp. 97-105, 2016. [CrossRef] [Google Scholar] [Publisher Link]

[11] Ghada M. Abo-Hamad et al., "Adaptive Mho Distance Protection for Interconnected Transmission Lines Compensated with Thyristor Controlled Series Capacitor," *Energies*, vol. 14, no. 9, pp. 1-29, 2021. [CrossRef] [Google Scholar] [Publisher Link]

[12] Juttu Tejeswara Rao, and Bhavesh R. Bhalja, "Prevention of Maloperation of Distance Relay under Severe Stressed Conditions for Series Compensated Transmission Line Considering Optimal Placement of Phasor Measurement Units," *IET Generation, Transmission & Distribution*, vol. 14, no. 11, pp. 2148-2159, 2020. [CrossRef] [Google Scholar] [Publisher Link]

[13] A.M. Abdullah, and K. Butler-Purry, "Secure Transmission Line Distance Protection during Wide Area Cascading Events Using Artificial Intelligence," *Electric Power Systems Research*, vol. 175, 2019. [CrossRef] [Google Scholar] [Publisher Link]

[14] Cholleti Sriram et al., "Improved Deep Neural Network (IDNN) with SMO Algorithm for Enhancement of Third Zone Distance Relay under Power Swing Condition," *Mathematics*, vol. 10, no. 11, pp. 1-19, 2022. [CrossRef] [Google Scholar] [Publisher Link]

[15] Shaik Abdul Gafoor, and P.V. Ramana Rao, "Wavelet Based Fault Detection, Classification and Location in Transmission Lines," *2006 IEEE International Power and Energy Conference*, Putra Jaya, Malaysia, pp. 114-118, 2006. [CrossRef] [Google Scholar] [Publisher Link]

[16] Yann Qi Chen, Olga Fink, and Giovanni Sansavini, "Combined Fault Location and Classification for Power Transmission Lines Fault Diagnosis with Integrated Feature Extraction," *IEEE Transactions on Industrial Electronics*, vol. 65, no. 1, pp. 561-569, 2018. [CrossRef] [Google Scholar] [Publisher Link]

[17] Alok Mukherjee, Palash Kumar Kundu, and Arabinda Das, "Transmission Line Faults in Power System and the Different Algorithms for Identification, Classification and Localization: A Brief Review of Methods," *Journal of the Institution of Engineers (India): Series B*, vol. 102, pp. 855-877, 2021. [CrossRef] [Google Scholar] [Publisher Link]

[18] Chao-Rong Chen, Cheng-Hung Lee, and Chi-Juin Chang, "Optimal Overcurrent Relay Coordination in Power Distribution System Using a New Approach," *International Journal of Electrical Power & Energy Systems*, vol. 45, no. 1, pp. 217-222, 2013. [CrossRef] [Google Scholar] [Publisher Link]

[19] Muhammad Usama et al., "A Comprehensive Review on Protection Strategies to Mitigate the Impact of Renewable Energy Sources on Interconnected Distribution Networks," *IEEE Access*, vol. 9, pp. 35740-35765, 2021. [CrossRef] [Google Scholar] [Publisher Link]

[20] Fadhel A. Albasri, Tarlochan Singh Sidhu, and Rajiv K. Varma, "Performance Comparison of Distance Protection Schemes for Shunt-FACTS Compensated Transmission Lines," *IEEE Transactions on Power Delivery*, vol. 22, no. 4, pp. 2116-2125, 2007. [CrossRef] [Google Scholar] [Publisher Link]

[21] Sayyed Mohammad Hashemi, Majid Sanaye-Pasand, and Mohammad Shahidehpour, "Fault Detection during Power Swings Using the Properties of Fundamental Frequency Phasors," *IEEE Transaction on Smart Grid*, vol. 10, no. 2, pp. 1385-1394, 2019. [CrossRef] [Google Scholar] [Publisher Link]

[22] Emil Bartosiewicz, Ryszard Kowalik, and Marcin Januszewski, "Overview and Test Results of Modern Pilot Schemes for Coordination of Line Distance Protection Relays," *2013 12th International Conference on Environment and Electrical Engineering*, Wroclaw, Poland, pp. 191-196, 2013. [CrossRef] [Google Scholar] [Publisher Link]

[23] A.A.A. Bakar et al., "A New Technique of Real-Time Monitoring of Fiber Optic Cable Networks Transmission," *Optics and Lasers in Engineering*," vol. 45, no. 1, pp. 126-130, 2007. [CrossRef] [Google Scholar] [Publisher Link]

[24] Aparna Kumari et al., "Blockchain-Based Peer-to-Peer Transactive Energy Management Scheme for Smart Grid System," *Sensors*, vol. 22, no. 13, pp. 1-19, 2022. [CrossRef] [Google Scholar] [Publisher Link]

[25] Muhammad Irfan, Seung-Ryle Oh, and Sang-Bong Rhe, "An Effective Coordination Setting for Directional Overcurrent Relays Using Modified Harris Hawk Optimization," *Electronics*, vol. 10, no. 23, pp. 1-18, 2021. [CrossRef] [Google Scholar] [Publisher Link]

[26] Sally El-Tawab, Hassan S. Mohamed, and A.M. Abdel-Aziz, "A Novel Proposed Algorithm to Enhance the Overcurrent Relays' Performance in Active Distribution Networks," *International Transactions on Electrical Energy Systems*, vol. 2022, pp. 1-16, 2022. [CrossRef] [Google Scholar] [Publisher Link]

[27] Yamen R. Alsyoufi, and Ammar A. Hajjar, "A High-Speed Algorithm to Discriminate between Power Swing and Faults in Distance Relays Based on a Fast Wavelet," *Electrical Power Systems Research*, vol. 172, pp. 269-276, 2019. [CrossRef] [Google Scholar] [Publisher Link]

[28] Bikash Patel, and Parthasarathi Bera, "Fast Fault Detection during Power Swing on a Hybrid Transmission Line Using WPT," *IET Generation Transmission Distribution*, vol. 13, no. 10, pp. 1811-1820, 2019. [CrossRef] [Google Scholar] [Publisher Link]

[29] Behrooz Taheri et al., "Detection of Power Swing and Fault Occurring Simultaneously with Power Swing Using Instantaneous Frequency," *Energy Systems*, vol. 11, no. 2, pp. 491-514, 2020. [CrossRef] [Google Scholar] [Publisher Link]

[30] Bikash Patel, "A New Technique for Detection and Classification of Faults during Power Swing," *Electrical Power Systems Research*, vol. 175, 2019. [CrossRef] [Google Scholar] [Publisher Link]

[31] A.M. Abdullah, and K. Butler-Purry, "Distance Protection Zone 3 Misoperation during System Wide Cascading Events: The Problem and a Survey of Solutions," *Electrical Power Systems Research*, vol. 154, pp. 151-159, 2018. [CrossRef] [Google Scholar] [Publisher Link]

[32] Behrooz Taheri, and Farzad Razavi, "Power Swing Detection Using RMS Current Measurements," *Journal of Electrical Enggineering and Technology*, vol. 13, no. 5, pp. 1831-1840, 2018. [CrossRef] [Google Scholar] [Publisher Link]

[33] Elmer Sorrentino, "Comparison of Five Methods of Compensation for Ground Distance Function and Assessment of Their Effect on the Resistive Reach in Quadrilateral Characteristics," *International Journal of Electrical Power & Energy Systems*, vol. 61, pp. 440-445, 2014. [CrossRef] [Google Scholar] [Publisher Link]